

Alma Mater Studiorum Università di Bologna  
Archivio istituzionale della ricerca

Shear strengthening of masonry wallettes resorting to structural repointing and FRCC composites

This is the final peer-reviewed author's accepted manuscript (postprint) of the following publication:

*Published Version:*

Casacci S., Gentilini C., Di Tommaso A., Oliveira D.V. (2019). Shear strengthening of masonry wallettes resorting to structural repointing and FRCC composites. CONSTRUCTION AND BUILDING MATERIALS, 206, 19-34 [10.1016/j.conbuildmat.2019.02.044].

*Availability:*

This version is available at: <https://hdl.handle.net/11585/689520> since: 2019-06-15

*Published:*

DOI: <http://doi.org/10.1016/j.conbuildmat.2019.02.044>

*Terms of use:*

Some rights reserved. The terms and conditions for the reuse of this version of the manuscript are specified in the publishing policy. For all terms of use and more information see the publisher's website.

This item was downloaded from IRIS Università di Bologna (<https://cris.unibo.it/>).  
When citing, please refer to the published version.

(Article begins on next page)

This is the final peer-reviewed accepted manuscript of:

**[Susanna Casacci, Cristina Gentilini, Angelo Di Tommaso and Daniel V. Oliveira. Shear strengthening of masonry wallettes resorting to structural repointing and FRCM composites. Construction and Building Materials. Vol. 206C, pp. 19-34, 2019]**

The final published version is available online at:  
**[<https://doi.org/10.1016/j.conbuildmat.2019.02.044>]**

Rights / License:

The terms and conditions for the reuse of this version of the manuscript are specified in the publishing policy. For all terms of use and more information see the publisher's website.

# Shear strengthening of masonry wallettes resorting to structural repointing and FRCM composites

Susanna CASACCI<sup>1,a</sup>, Cristina GENTILINI<sup>2,b\*</sup>, Angelo DI TOMMASO<sup>1,b</sup>, and Daniel V. OLIVEIRA<sup>3,d</sup>

<sup>1</sup>*Department of Civil, Chemical, Environmental and Materials Engineering – DICAM  
University of Bologna, Viale del Risorgimento 2, 40136 Bologna, Italy*

<sup>2</sup>*Department of Architecture – DA*

*University of Bologna, Viale del Risorgimento 2, 40136 Bologna, Italy*

<sup>3</sup>*ISISE, University of Minho, Department of Civil Engineering, Guimarães, Portugal*

<sup>a</sup>susanna.casacci@unibo.it; <sup>b</sup>cristina.gentilini@unibo.it; <sup>c</sup>angelo.ditommaso@unibo.it; <sup>d</sup>danvco@civil.uminho.pt

\*corresponding author

## Abstract

Results of an experimental campaign conducted on plain and reinforced masonry wallettes subjected to diagonal compression tests are presented in this paper. The masonry panels were reinforced by means of two strengthening techniques: structural repointing achieved by inserting basalt bars in the mortar bed joints and fiber reinforced cementitious matrix (FRCM) composite, obtained by applying a single-ply glass mesh on the sides of the specimens. The structural effects of symmetric and asymmetric strengthening configurations are investigated. The main mechanical parameters, such as shear capacity, ductility and shear modulus, are compared and discussed introducing a calibrated reinforcement ratio. Further, analytical procedures presented in the codes and in literature are followed to predict the shear capacity of the unstrengthened and strengthened wallettes and, finally, compared to the values obtained experimentally.

**Keywords:** Repointing; masonry; diagonal compression test; lime-based matrix; basalt bars; FRCM; glass mesh.

## Nomenclature list

Symbol	Definition
$A_b$	Average bond area between the matrix and the bar
$A_{FRCM}$	Area of FRCM reinforcement by unit width in both directions (horizontal and vertical)
$A_{BAR}$	Cross-sectional area of the bar
$A_m$	Interface loading area between the steel shoe and the wall
$A_n$	Net cross-sectional area of the wallette
$E$	Elastic modulus
EB	Externally bonded
$E_{BAR}$	Elastic modulus of the bar
$E_{FRCM}$	Elastic modulus of the FRCM
$E_m$	Elastic modulus of masonry

$f_{cb}$	Compressive strength of the bricks
$f_{cm}$	Compressive strength of the mortar
$f_{fm}$	Flexural strength of the mortar
$f_i$	Force carried by $i$ -th bar
$f'_m$	Compressive strength of masonry
$f_{t,BAR}$	Tensile strength of the bar
$f_{t,FRCM}$	Tensile strength of the FRCM
$f'_t$	Tensile strength of masonry
FRCM	Fiber reinforced cementitious matrix
FRP	Fiber reinforced polymer
$\phi_{BAR}$	Diameter of the bar
$g$	Gage length
$G$	Shear modulus
$h$	Height of the brick
$H$	Height of the masonry panel
$L_e$	Effective length of the bar
$L_i$	Effective bond length of the $i$ -th bar
$n$	Percentage of the gross area of the unit brick that is solid
$n_{layer}$	Number of layer of fabric
NSM	Near surface mounted
PBO	Polyparaphenylene benzobisoxazole
$P$	Applied load
$P_{max}$	Maximum applied load
$P_{max}^{UNR}$	Maximum applied load for the unreinforced specimen
$P_{max}^R$	Maximum applied load for the reinforced specimen
$R_{BAR}$	Radius of the bar
RF-A	Specimen reinforced by single-ply asymmetric FRCM system
RF-S	Specimen reinforced by single-ply symmetric FRCM system
RR-A	Specimen reinforced by asymmetric structural repointing
RR-S	Specimen reinforced by symmetric structural repointing
$t$	Thickness of the brick
$t_m$	Thickness of the mortar joint
$T$	Thickness of the masonry panel
$u$	Horizontal displacement
URM	Unreinforced masonry specimen
$v$	Vertical displacement
$V_n$	Shear capacity
$V_c$	Shear capacity due to toe crushing failure
$V_{dt}$	Shear capacity due to diagonal tension failure

$V_f$	Contribution of reinforcement to shear capacity of the specimen
$V_m$	Shear capacity of the unreinforced masonry wall
$V_{sf}$	Shear capacity due to shear friction failure
$V_{ss}$	Shear capacity due to shear sliding failure
$w$	Width of the brick
$W$	Width of the masonry panel
$\theta$	Angle between horizontal and the main diagonal of the wall
$\mu$	Pseudo-ductility
$\mu_m$	Modified coefficient of internal shear friction in mortar joint
$\mu_0$	Coefficient of internal friction in the mortar joints
$\gamma$	Shear strain
$\varepsilon_{BAR}$	Breaking elongation of the bar
$\varepsilon_{FRCM}$	Ultimate tensile strain of the FRCM
$\Delta$	Structural enhancement achieved in terms of $P_{max}$ by using reinforcement
$\Delta u$	Horizontal extension of the specimen
$\Delta v$	Vertical shortening of the specimen
$\rho_f$	Calibrated reinforcement ratio
$\tau$	Shear stress
$\tau_{el}$	Shear stress in the elastic branch
$\tau_{max}$	Maximum shear stress
$\tau_b$	Average shear bond strength between the matrix and the bar
$\tau_0$	Shear bond strength of mortar joints
$\tau_{0,m}$	Modified shear bond strength of mortar joints

28

## 29 **1. Introduction**

30 Masonry buildings constitute the greatest part of the building stock in Europe. It is well known that masonry  
31 structures suffer from several structural deficiencies. Low ductility, low mechanical properties (in particular,  
32 a poor tensile strength), as well as weak connections between structural elements, are among the causes of the  
33 high vulnerability against out-of-plane loads and of the fragile collapse of masonry structures [1-3]. For these  
34 reasons, strengthening interventions are often necessary to improve the mechanical performance of masonry  
35 structures [4, 5]. Innovative materials, as externally bonded (EB) textiles such as FRPs (fiber reinforced  
36 polymers) have been used for repairing and strengthening both modern and historic constructions and structural  
37 components [6, 7]. The composite materials are used to: (i) provide tensile strength to masonry elements; (ii)  
38 modify the mechanical behaviour and the collapse mechanisms of the structure and (iii) increase the structure  
39 displacement capacity, [8].

40 Recently, fiber reinforced cementitious matrix (FRCM) composites have been introduced in order to overcome  
41 well-known drawbacks of FRP composites such as low compatibility with masonry substrates, low  
42 reversibility of the interventions, low vapor permeability and durability issues against environmental factors,

[9]. FRCM composites are a combination of inorganic matrices and high-strength fibers namely steel, carbon, polyparaphenylene benzobisoxazole (PBO), basalt or glass [10-12]. The inorganic matrix exhibits significant heat resistance, can be applied at low temperatures or on wet surfaces and allows vapor permeability [13]. Additionally, FRCM composites can be easily removed in case they need to be substituted [14].

In the case of masonry façades or elements with fair-faced bricks, the use of EB composites for retrofitting interventions may not represent a viable solution, because it can violate aesthetic and conservation requirements. For this reason, the so-called reinforced repointing technique has been developed, being minimally invasive and respectful of the aesthetic of fair-faced masonry elements, [15-18]. The reinforced repointing technique involves the application of materials having high tensile strength such as glass or steel bars, carbon wires, steel textile sheets or composite thin pultruded laminae, to reduce the vulnerability of masonry structures against in-plane actions and long-term high-level dead loads, [19-21]. The technology is also called near surface mounted (NSM) reinforcement [22], because the reinforcing material is embedded with a filler (typically epoxy paste or cement grout) in the horizontal bed joints of a wall previously grooved for few centimetres, usually by means of a grinder.

In order to check for the structural effectiveness of FRCM composites and NSM bars applied to masonry for in-plane loading, reinforced masonry panels are commonly subjected to diagonal compression tests. In the last decade, several studies have been published on masonry reinforced with EB FRCM systems subjected to diagonal compression. In [23], masonry panels reinforced with a carbon fiber mesh embedded in a cementitious mortar matrix were subjected to both monotonic and cyclic in-plane loading. The strengthening system provided an increase of both shear strength and energy dissipation. Incerti et al. [24] performed diagonal compression tests on brick double-wythe masonry panels characterized by different textures, as flemish bond and header bond. The panels were reinforced using the same strengthening system, i.e. a basalt bi-directional grid coupled with a lime-based mortar matrix. Results confirmed the efficiency of FRCM composites in improving the shear behavior of masonry panels.

In [25], masonry walls reinforced with glass FRCM (GFRCM) were tested. The GFRCM compounds were able to increase the load capacity of the walls and demonstrated a high bond with the masonry surface, reducing the need of transversal ties. An investigation of the in-plane behavior of single- and double-sided strengthened masonry wall panels with a multiaxial hybrid glass-polypropylene fabric coated in a natural hydraulic lime-based mortar was undertaken in [26]. The experimental program considered both solid clay-bricks and hollow clay-blocks as masonry substrate. Recently, different attempts were made to employ natural fibers instead of synthetic ones, as in [27], where the behaviour of tuff masonry specimens strengthened with a textile made with hemp fibers embedded in a lime-based mortar matrix loaded under diagonal compression was investigated. Sisal fibers were employed to strengthen masonry panels against in-plane loading in [28].

From the brief literature review carried out above, walls strengthened with FRCM evidenced significant improvements in strength and ductility. However, it emerges that FRCM composites can be applied using a great number of different fiber types (synthetic or natural) embedded in inorganic matrices of different nature (e.g. cementitious-based or lime-based), as well as using different strengthening layouts (symmetric or asymmetric

configuration), on different masonry typologies (single or double-wythe, made of solid bricks or hollow blocks, employing natural stones or artificial bricks).

Due to the growing interest for FRCM composites and the extremely high combination of variables associated with its use, a wide experimental and analytical research activity is needed to quantify their contribution to load carrying capacity and ductility enhancement as a function of the typology of the substrate, as well as of the mortar matrix and fiber types.

Additionally, studies on masonry panels reinforced with basalt NSM bars embedded in a lime-based matrix, as the one herein proposed, are very limited, since the available research programs were carried out on masonry walls made of concrete blocks reinforced using carbon or glass bars (see Section 2).

It should also be noted that FRCM and NSM composites usually exhibit scattered results. The variability is due to several factors: the built-in variability of the masonry and of the matrix, and as a consequence, its mechanical behavior is strongly dependent on casting and curing conditions, as well as on substrate conditions. This aspect represents a limit for this class of composites with respect to FRPs, where the variability is mainly related to the masonry substrate. For these reasons, experimental works on masonry reinforced with FRCM composites or NSM bars are necessary to fully characterize their mechanical behaviour. The aim of the present work is to contribute in deepening the knowledge on this topic by enriching the limited existing literature.

Given the context above, the present paper discusses the results of an experimental program involving small masonry specimens made of fire-clay bricks and lime-based mortar subjected to diagonal compression loading. After curing, specimens were reinforced using two different strengthening solutions: a group of specimens was strengthened with basalt bars by using the NSM reinforcement technique. To the second group of specimens, a FRCM system, consisting of a 1-ply glass mesh and hydraulic lime-based mortar was applied. Symmetrical and asymmetrical configurations were considered for both retrofitting techniques in order to observe the influence of the reinforcement eccentricity: this condition is important in in-field applications, since most of the times only one side of the wall can be strengthened. Results are presented in terms of load capacity, shear modulus as well as ductility. In order to compare the results obtained from the experimental tests, a calibrated reinforcement ratio is defined. Finally, analytical procedures presented in the codes and in literature are followed to predict the shear capacity of the unreinforced specimens. The shear contribution of the NSM bars is calculated following a modified approach presented in [29], while for the FRCM system contribution, ACI 549 Standard [30] is adopted.

The paper is organised as follows. Section 2 presents a brief summary on previous diagonal tests conducted on NSM strengthened masonry walls. Materials, specimens and test set-up employed in the experimental program are presented in Section 3. Results of the experimental campaign are collected and discussed in Section 4. In Section 5, analytical procedures to compute shear capacities of both unreinforced and reinforced specimens are presented and compared to the experimental values. Some final considerations conclude the paper.

## **2. Previous tests on NSM bars in masonry subjected to diagonal compression**

In this section, the main recent results of experimental campaigns conducted on masonry specimens reinforced by means of NSM bars and subjected to diagonal compression are reported. Results are collected in Table 1 in terms of slenderness ratio, defined as the ratio between the height and the thickness of the panel, masonry and reinforcement properties, shear capacity and increase in shear capacity with respect to the unreinforced specimens. In order to compare the results, a calibrated reinforcement ratio  $\rho_f$ , which represents the ratio between the axial stiffness of the reinforcement and that of masonry, is introduced [31, 32]:

$$\rho_f = \frac{A_{rein}}{A_n} \frac{E_{rein}}{E_m} 100\% \quad (1)$$

where  $A_{rein}$  is the area of the reinforcement,  $A_n$  is the net masonry area, while  $E_{rein}$  and  $E_m$  are the moduli of elasticity of the reinforcing material and masonry, respectively.

To the authors' knowledge, the most recent contribution on this topic is the work by Yu et al. [33], which tested eight concrete masonry specimens strengthened with prestressed GFRP bars. The bars were inserted in the mortar joints by means of epoxy paste, following different schemes. The main aspects investigated in the paper were the effect of the bar prestress level and the reinforcement ratio on the load carrying capacity of the specimens. Results showed an increase of the shear capacity of the reinforced walls with prestressed bars with respect to both URM control specimens and specimens reinforced with NSM bars without prestress. URM walls were characterized by a stair-stepped central crack, while the presence of the bars changed the failure mode from shear friction to a combination of shear sliding and friction, or to shear sliding along a single bed joint. It is shown that an increase of the reinforcement ratio or of the level of prestress in the bars did not lead to a proportional increment in the load carrying capacity.

Dizhur et al. [34] tested clay brick wall panels reinforced using NSM CFRP strips. NSM strips were inserted vertically or following a cross pattern in the specimens, thus they were not inserted in the mortar bed joints. This solution resulted in an improved structural performance of the retrofitted masonry panels when compared to the control units. However, this application is not interesting to the aim of the present study, since in general, the vertical insertion of the bars does not represent an acceptable solution in the case of historic or monumental buildings due to strict preservation criteria that have to be usually observed.

Ismail et al. [35] investigated the diagonal shear behavior of 17 masonry wallettes strengthened using NSM helical steel bars. Both single and double-wythe panels were tested, considering horizontal, vertical and grid patterns of reinforcement. Three out of 17 specimens were reinforced embedding the steel bars in the mortar bed joints that were inserted in the slots employing a cementitious grout. Results showed that single-wythe thick wallettes reinforced with the horizontal NSM bars registered a decrease in shear strength. This was attributed to the fact that the masonry bond strength for these specimens resulted significantly lower with respect to the series average value. However, even if no shear strength increase was recorded, a large increment in pseudo-ductility was observed with respect to URM walls.



151 Mahmood and Ingham [36] performed diagonal compression tests on 17 double-wythe solid clay brick  
 152 masonry wallettes. Some wallettes were retrofitted by applying EB glass fabrics and others by using NSM  
 153 CFRP rectangular bars. Also in this campaign, vertical, horizontal and a combination of horizontal and vertical  
 154 bars were considered among the different retrofitting solutions. CFRP bars were embedded in the slots by  
 155 means of an epoxy paste. Results showed that symmetric and asymmetric applications of NSM horizontal bars  
 156 lead to a similar increase in shear strength, even if the symmetrically reinforced panel was characterized by a  
 157  $\rho_f$  that was double with respect the asymmetric one.

158 In the paper by Tumialan et al. [37] six walls made of hollow concrete blocks and reinforced with glass FRP  
 159 (GFRP) bars embedded into an epoxy-based paste were tested. A remarkable increase in shear capacity,  
 160 ranging between 30% and 80%, was achieved. The wall specimen, where only one face was strengthened,  
 161 showed the same increase in shear strength as the one with the same amount of reinforcement ratio but  
 162 symmetrically distributed, while the wall with half amount of reinforcement registered less than half of increase  
 163 in load carrying capacity. The authors stated that the results obtained for the concrete walls should not be  
 164 generalized for walls with clay bricks, which are characterized by different mechanical and geometrical  
 165 properties.

166 Turco et al. [38] present experimental results of different applications of NSM bars for the shear reinforcement  
 167 of masonry walls. Different strengthening combinations were considered: smooth and sand-coated glass FRP  
 168 bars as reinforcement, epoxy paste and latex modified cementitious paste as groove filling materials. All the  
 169 retrofitted specimens registered an increase in shear capacity (up to 120%) and ductility. Some specimens  
 170 showed an out-of-plane phase during failure, in particular the walls strengthened by using the sand-coated bars  
 171 with epoxy paste due to the high stiffness of the reinforcement. No out-of-plane component was observed for  
 172 the specimens where low-bond systems were employed: the lower stiffness of reinforcement allowed some  
 173 slip and, consequently, a better redistribution of stresses was possible.

174 It should be noted that in almost all the studies considered above, only one specimen per type was tested (in  
 175 few exceptions two panels per type were tested) and only few studies deal with NSM bars inserted in mortar-  
 176 filled grooves. Additionally, it can be observed that a lot of variables are involved in the case of NSM bar  
 177 strengthening of masonry: the masonry substrate typology, the reinforcement type, the groove filling material  
 178 type, the bar cross-sectional shape, the presence of prestress in the reinforcement as well as the pattern  
 179 distribution of the reinforcement. This large number of parameters requires extensive laboratory  
 180 characterization and testing to get insight in the mechanical behaviour, to assess existing analytical procedures  
 181 and to address new design provisions.

Table 1. Summary of recent diagonal compression tests on masonry panels reinforced by using NSM bars.

Reference	Masonry panel properties				NSM reinforcement				Shear capacity [KN]	Shear strength increase with respect to URM (%)		
	Material		Dimensions [mm] (W × H × T)	Slenderness ratio [l]	Number of tested panels for each type	Material	Filling material	Pattern			Reinforcement ratio $\rho_f$ (%)	
Yu et al. [33]	Hollow concrete blocks	W1, W2	1630 × 1630 × 150	10.87	2	/	/	/	0	112.3	/	
		W3			1	3 GFRP bars ( $\phi 6$ )	Two-component general purpose epoxy resin	Horizontal (1 face)	0.40	187.7	67	
		W4				7 GFRP bars ( $\phi 6$ )			0.93	224.2	100	
		W5				2 Prestressed GFRP bars ( $\phi 6$ )			0.27	195.7	74	
		W6				3 Prestressed GFRP bars ( $\phi 6$ )			0.40	210.8	88	
		W7				4 Prestressed GFRP bars ( $\phi 6$ )			0.53	210.8	88	
		W8				7 Prestressed GFRP bars ( $\phi 6$ )			0.93	234.9	109	
		Ismail et al. [35]				New solid clay bricks			W1C-1	1200 × 1200 × 110	10.91	1
W1S-7, W1S-8	2		7 High strength twisted stainless steel bars ( $\phi 6$ )	Thixotropic injectable grout	Horizontal (2 faces)		0.19	114.5	-27			
Salvaged solid clay bricks	W2C-3		1200 x 1200 x 220	5.45	1	/	/	/	0	51.0	/	
	W2S-14					2 High strength twisted stainless steel bars ( $\phi 6$ )	Thixotropic injectable grout	Horizontal (1 face)	0.08	71.6	40	
Mahmood and Ingham [36]	Solid clay bricks		AP8	1170 × 1175 × 225	4.78	1	/	Two-component epoxy resin	/	0	37.0	/
		WTC8	5 CFRP rectangular bars (1.2 mm x 15 mm)				Horizontal (1 face)		0.74	65.0	76	
		WTC9	10 CFRP rectangular bars (1.2 mm x 15 mm)				Horizontal (2 faces)		1.48	67.0	81	
Tumialan et al. [37]	Hollow concrete blocks	Wall 1	1625 × 1625 × 152	10.69	1	/	Epoxy-based paste	/	0	108.09	/	
		Wall 2				14 GFRP bars ( $\phi 6.25$ )		Horizontal (1 face)	0.82	197.5	82	
		Wall3						Horizontal (2 faces)	0.82	194.83	80	
		Wall 4				6 GFRP bars ( $\phi 6.25$ )		Horizontal (1 face)	0.35	139.23	28	
Turco et al. [38]	Concrete blocks	Control	1600 × 1600 × 150	10.6	1	/	Epoxy-based paste	Horizontal (1 face)	n.d.(*)	108	/	
		E-6CG-1HJ				7 sand coated GFRP bars ( $\phi 6.35$ )				198.9	84	
		E-5SG-1HJ				7 smooth GFRP bars ( $\phi 5$ )				241.1	123	
		C-6CG-1HJ				7 sand coated GFRP bars ( $\phi 6.35$ )				Latex modified cementitious paste	184.1	70
		E-6CG-2HJ				4 sand coated GFRP bars ( $\phi 6.35$ )				Epoxy-based paste	195	81
		E-5SG-2HJ				4 smooth GFRP bars ( $\phi 5$ )					190.4	76
		E-6CG-2HJB				8 sand coated GFRP bars ( $\phi 6.35$ )					189	75
		n.d.(*) not deducible from the paper since some data are missing										

### 3. Materials and methods

#### 3.1. Bricks and mortars

Standard tests were performed to characterize the mechanical properties of the materials used in the experimental campaign. Portuguese solid clay bricks having nominal size of  $200 \times 100 \times 50 \text{ mm}^3$  were used for manufacturing the wallettes. Brick compressive strength in flatwise direction was obtained according to EN 772-1 [39] on six 40 mm cubic specimens.

Two different types of commercial pre-mixed mortars were used for the preparation of the specimens. A lime-based mortar (mortar A), classified as M5 according to EN 998-2 [40], was used to build the specimens. The mortar was prepared following the instructions provided by the manufacturer, i.e. mixing 4 liters of clean water with 25 kg of powder, [41]. From the same batch of mortar used for the joints, 26 prismatic samples of nominal size  $40 \times 40 \times 160 \text{ mm}^3$  were cast and cured at laboratory conditions for two months. After curing, prismatic samples were tested in order to determine compressive and flexural strengths according to EN 1015-11 [42]. The testing age of the mortar was approximately the same as the one of the wallettes.

The mortar employed for the strengthening operations (referred as mortar B throughout this paper) was a bi-component commercially available, based on natural hydraulic lime and pozzolanic fraction, and classified as M15 according to EN 998-2 [40]. The mixing ratio was a drum of component two for every 25 kg of component one [43]. Using mortar B, Dalalbashi et al. [44] performed compressive and flexural tests according to [42, 45] on five prismatic specimens, at different ages. Tests were performed in a universal testing machine at a rate of 10 N/s. The compressive and flexural strengths at 28 days of curing are reported in this paper, since changes in the mechanical properties after the first 30 days were not significant.

In Table 2, mechanical properties of bricks and mortars are listed in terms of brick compressive strength  $f_{cb}$ , as well as compressive  $f_{cm}$  and flexural strength  $f_{fm}$  of mortars A and B. The elastic modulus  $E$  of mortar B provided by the manufacturer is reported as well.

#### 3.2. Basalt bars and glass mesh

In order to assess the mechanical properties of the basalt bars used to strengthen the specimens, direct tensile tests were performed, Fig. 1a. An anchorage system consisting of steel pipes filled with a thixotropic bi-component epoxy resin was employed. The dimension of the specimens was derived according to ASTM D7205 [46]. The specimens, with a total length of 1000 mm, were provided with two anchoring systems of 300 mm long each. Diameter  $\phi_{BAR}$  and cross-sectional area  $A_{BAR}$  resulted equal to 5.50 mm (CoV=1%) and  $23.76 \text{ mm}^2$ , respectively.

A universal testing machine was used for the tests. The top end pipe was encased in a steel frame connected to the top jaw of the machine. The gripping mechanism of the upper frame, as shown in Fig. 1b, allowed for torsional rotation to avoid the negative effects of possible eccentricity and misalignments of the specimens. The bottom end pipe was encased in a steel frame fixed to the lower grip of the testing machine. Each specimen was provided with a clip gauge (length equal to 100 mm) placed in the central position of the bar to record the elongation and the load was applied at a constant speed of 2 mm/min until the failure of the specimen. A total

of four bars were tested. In Fig. 1c, a bar at failure is reported, while in Fig. 1d, the stress-strain curves for the tested bars are shown. Stress-strain curves are linear till the peak load, showing a brittle failure of the bars. In Table 2, the tensile strength  $f_{t,BAR}$ , elastic modulus  $E_{BAR}$ , and breaking elongation  $\varepsilon_{BAR}$ , as obtained from the tests, are reported.

The mesh used to strengthen the specimens consisted of an alkali-resistant pre-primed glass fiber mesh, characterized by a  $25 \times 25 \text{ mm}^2$  grid spacing, [47]. Equivalent thickness of the fiber grid and fiber area per unit width are equal to 0.035 mm and  $35.27 \text{ mm}^2/\text{m}$ , respectively [47]. Its linear tensile strength, modulus of elasticity and elongation at failure are reported in Table 2. Leone et al. [48] tested FRCM coupons in order to obtain the stress-strain curve and the main mechanical properties of the composite according to the test method presented in [49]. Coupons with different sizes and testing ages were tested. Due to the variability of the results, average experimental values were reported in this study. The cracked elastic modulus of the FRCM  $E_{FRCM}$ , the ultimate tensile strain  $\varepsilon_{FRCM}$ , and the ultimate tensile stress  $f_{u,FRCM}$  that have to be used in the analytical calculations are reported in Table 2.

Table 2. Mechanical properties of the materials used in the experimental tests.

Sub-system	Material	Mechanical property	Average value	CoV (%)
Walette	Fire-clay brick	Compressive strength $f_{cb}$ [MPa]	14.3	4
	Bedding mortar (mortar A)	Compressive strength $f_{cm}$ [MPa]	5.8	27
		Flexural strength $f_{fm}$ [MPa]	2.6	24
Strengthening	Matrix (mortar B)	Compressive strength $f_{cm}$ [MPa]	7.07 <sup>a</sup>	10.5
		Flexural strength $f_{fm}$ [MPa]	4.71 <sup>a</sup>	7.8
		Elastic modulus $E$ [MPa]	8000 <sup>b</sup>	-
	Basalt bar	Tensile strength $f_{t,BAR}$ [MPa]	777.3	2
		Elastic modulus $E_{BAR}$ [MPa]	34180	2
		Breaking elongation $\varepsilon_{BAR}$ [%]	2.1	6
	Glass mesh	Linear tensile strength [kN/m]	45 <sup>b</sup>	-
		Elastic modulus [MPa]	72000 <sup>b</sup>	-
		Breaking elongation [%]	1.8 <sup>b</sup>	-
	FRCM coupon	Elastic modulus in the cracked phase $E_{FRCM}$ [MPa]	40500 <sup>c</sup>	-
		Ultimate tensile strain $\varepsilon_{FRCM}$	0.0098 <sup>c</sup>	-
		Ultimate tensile stress $f_{u,FRCM}$ [MPa]	853.5 <sup>c</sup>	-

<sup>a</sup>value from [44], <sup>b</sup>value provided by the manufacturer, <sup>c</sup>value from [48]

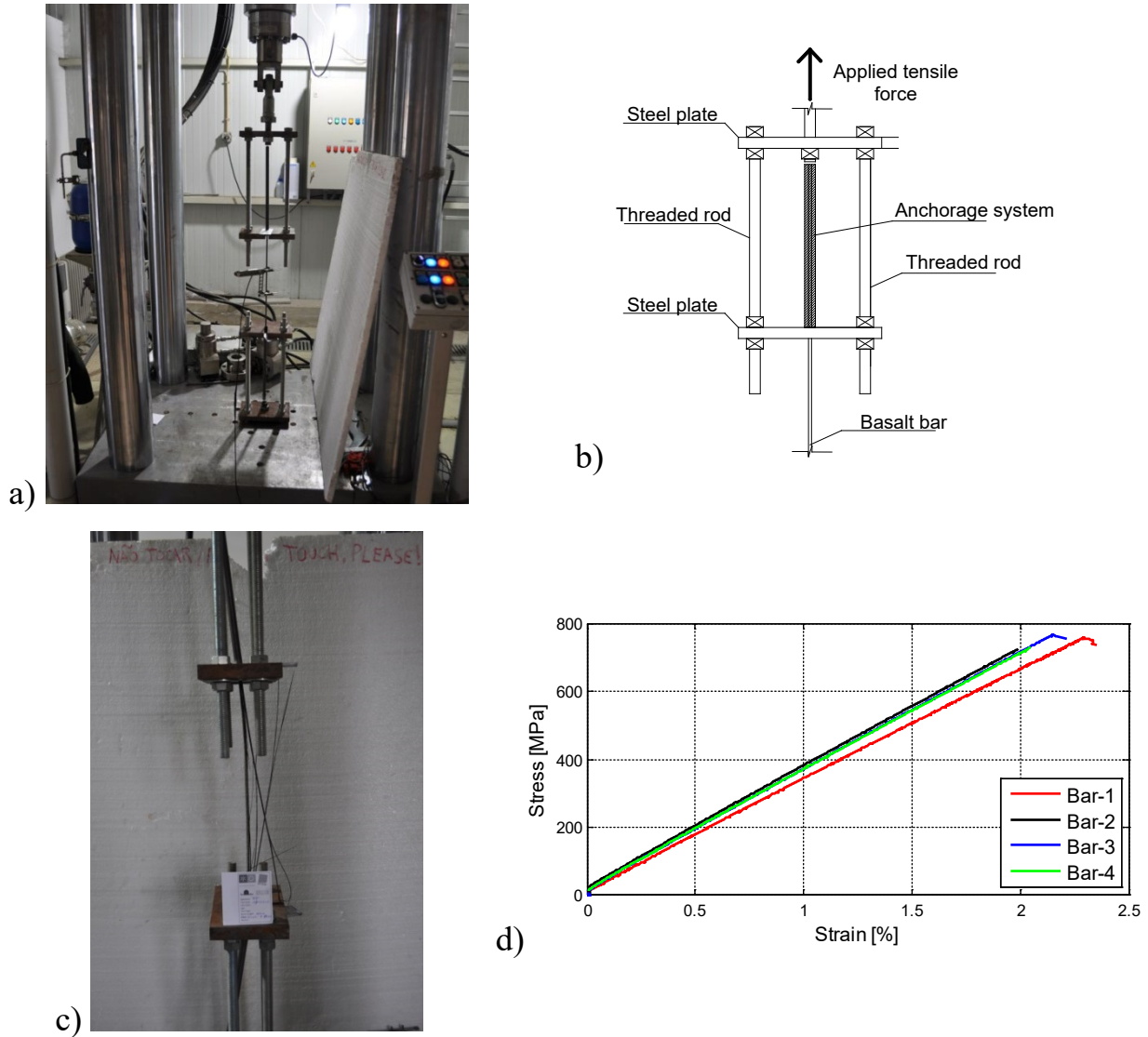


Fig. 1. Basalt bars: a) direct tensile test, b) detail of the top gripping mechanism of the bar, c) failure mode; d) stress-strain curves.

### 3.3. Masonry wallettes

Each masonry specimen was built with nine courses of bricks and eight 10 mm thick mortar layers, and had a nominal total size equal to  $520 \times 530 \times 100 \text{ mm}^3$ , see Fig. 2. The dimensions of the specimens were defined taking into account their weight, handling procedures and acceptable slenderness in order to avoid instability issues, which in this case was equal to 5.3 [24, 50]. In particular, five types of specimens were prepared, as follows:

- i) reference unreinforced specimens hereinafter denoted as URM, Fig. 2;
- ii) strengthened specimens with asymmetric structural repointing obtained by inserting one basalt bar in the third and in the sixth mortar joints for a total of two bars, hereinafter denoted as RR-A, Fig. 3;
- iii) strengthened specimens with symmetric structural repointing obtained by inserting two basalt bars in the third and two in the sixth mortar joints for a total of four bars, hereinafter denoted as RR-S, Fig. 3;

252 iv) strengthened specimens with asymmetric FRCM obtained applying a 1-ply glass mesh on one side of the  
253 specimen, hereinafter denoted with RF-A, Fig. 4;

254 v) strengthened specimens with symmetric FRCM obtained applying a 1-ply glass mesh on each side of the  
255 specimen (characterized by an amount of reinforcement that is twice with respect to RF-A), hereinafter denoted  
256 as RF-S, Fig. 4.

257 Strengthening operations were carried out after 28 days of curing of the wallettes at laboratory conditions. The  
258 main phases of the repointing process consisted in the preparation of the grooves in the selected mortar joints  
259 for a depth around 20 mm from the edges by means of a grinder. The grooved joints were cleaned with an air  
260 gun and wet manually with a sprinkler. They were partially filled with structural mortar (mortar B) and the  
261 bars were placed and pushed in the mortar such that the mortar surrounded the bars. Afterwards, the grooves  
262 were completely filled with a second layer of structural mortar, finally restoring the wall original appearance,  
263 Fig. 3.

264 For the application of the FRCM composite, the following operations were conducted:

265 1) the surfaces of the panels to be reinforced with FRCM composite were manually wet by means of a sprinkler;  
266 2) after the wetting of the surface, mortar B was thrown manually with a metallic trowel on the surface in order  
267 to increase the surface roughness and consequently the adhesion between the surface of the wall and the first  
268 mortar layer used to apply FRCM composite;

269 3) afterwards, a uniform layer of mortar B (approximately 4-5 mm-thick) was applied manually on the surface  
270 using a flat trowel;

271 4) while the product was still fresh, the glass mesh was pressed lightly on it with a flat trowel so that it adhered  
272 perfectly to the mortar;

273 5) then, a second uniform layer of mortar B (approximately 4-5 mm-thick) was applied manually using a flat  
274 trowel in order to completely cover the glass mesh;

275 6) the surface was smoothed while still fresh.

276 All the NSM and FRCM reinforced wallettes were left to cure till the time of testing. Table 3 summarizes the  
277 different masonry specimens that were built. Three wallettes for each category were prepared, thus totalizing  
278 15 specimens.

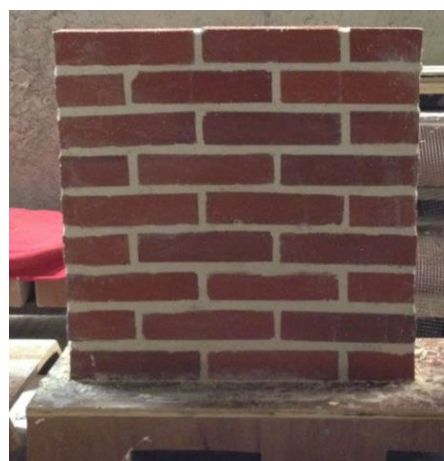
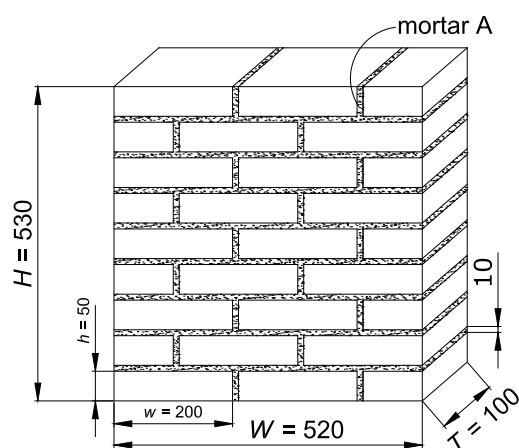
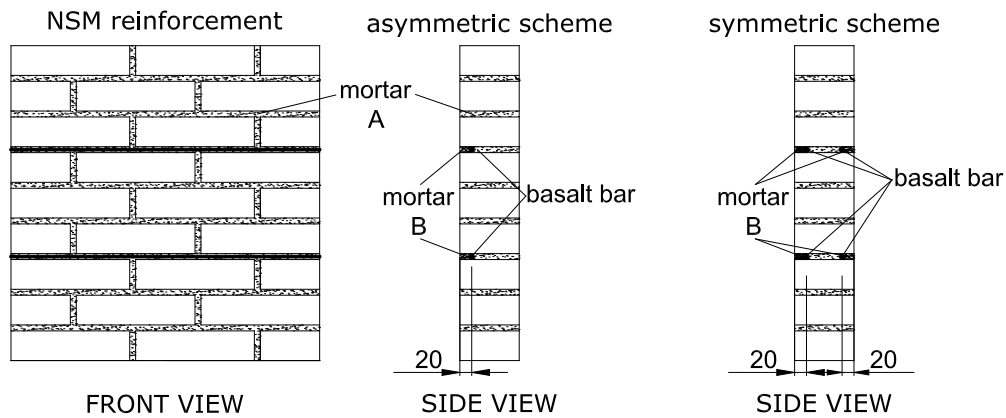


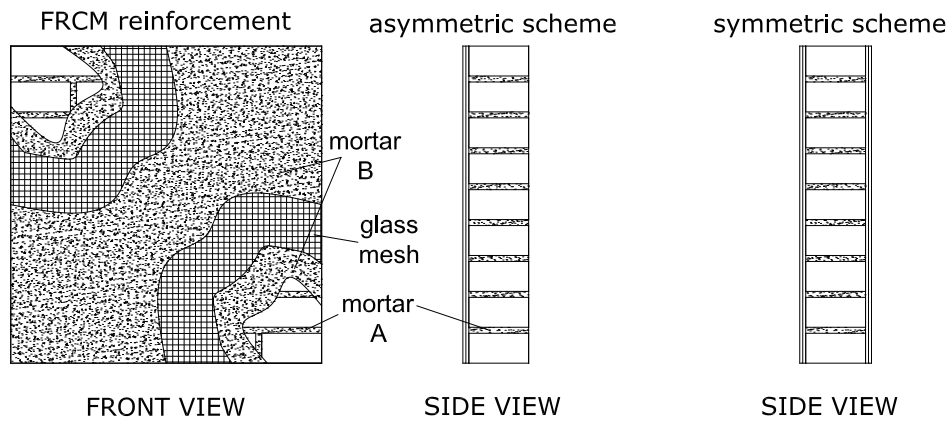
Fig. 2. Unreinforced masonry specimens (URM). Sizes in mm.

281



282

283 Fig. 3. Reinforced masonry wallettes with NSM basalt bars: asymmetric reinforcement scheme (RR-A  
284 specimens) and symmetric reinforcement scheme (RR-S specimens). Sizes in mm.



285

286 Fig. 4. Reinforced masonry wallettes with FRCM technique: asymmetric reinforcement scheme (RF-A  
287 specimens) and symmetric reinforcement scheme (RF-S specimens). Sizes in mm.

288

289 Table 3. Specimen labels and description.

Specimen label	Description	Number of tested specimens
URM	Unreinforced specimen (Fig. 2)	3
RR-A	Reinforced specimen: 2 basalt bars inserted asymmetrically in the mortar joints (Fig. 3)	3
RR-S	Reinforced specimen: 4 basalt bars inserted symmetrically in the mortar joints (Fig. 3)	3
RF-A	Reinforced specimen: 1-ply glass-based FRCM composite applied asymmetrically on one side (Fig. 4)	3
RF-S	Reinforced specimen: 1-ply glass-based FRCM composite applied symmetrically on both sides (Fig. 4)	3

290

### 3.4. Test set-up and instrumentation

After curing, all wallette specimens were subjected to a diagonal compression test [51], see also Fig. 5a. The load was applied through steel shoes with dimensions of  $115 \times 115 \times 15 \text{ mm}^3$  placed at diagonally opposing bottom and top corners. All specimens were tested in a universal testing machine of 500 kN load capacity operated under displacement control at a rate equal to  $2 \text{ }\mu\text{m/s}$ .

In Fig. 5b and Fig. 5c, the instrumentation of the specimens is shown. During the test, the values of the applied load and of the diagonal displacements were recorded. The displacements were measured by four LVDTs: two applied on the front face (LVDT<sub>c,f</sub> and LVDT<sub>t,f</sub>), and two on the back face, (LVDT<sub>c,b</sub> and LVDT<sub>t,b</sub>). In particular, LVDT<sub>c,f</sub> and LVDT<sub>c,b</sub> were vertically oriented along the force line to measure the wall shortening, while LVDT<sub>t,f</sub> and LVDT<sub>t,b</sub> were placed horizontally, perpendicular to the force line to record the crack opening. A load cell was used to measure the force,  $P$ , along the loaded diagonal.

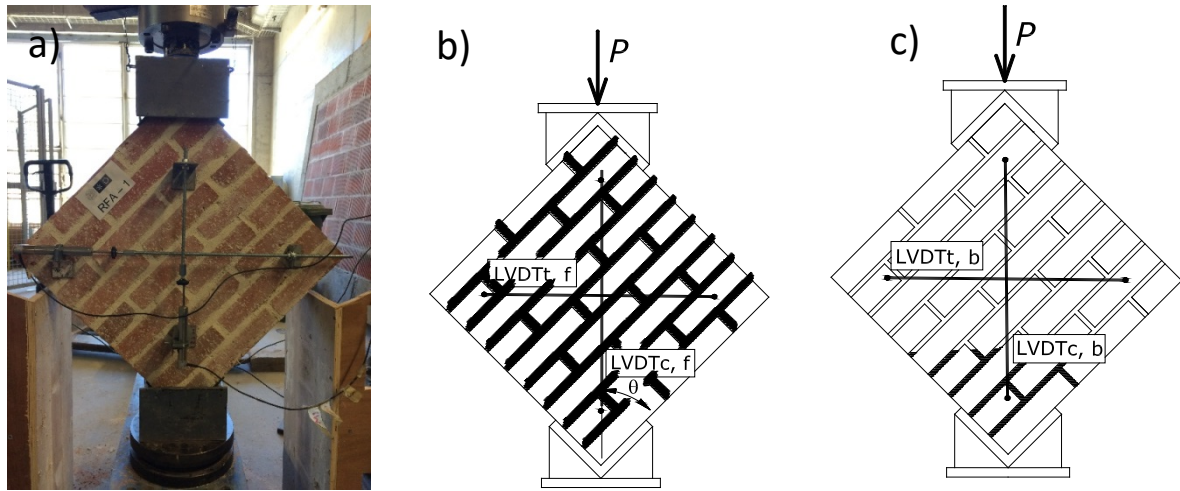


Fig. 5. Diagonal compression test: a) set-up, b) instrumentation of the front face; c) instrumentation of the back face.

## 4. Experimental results

### 4.1. Shear stress-strain curves

In the following, results obtained from the tests conducted on the specimens are presented. In particular, results are given in terms of shear stress ( $\tau$ ) versus shear strain ( $\gamma$ ). Following ASTM E519 [51],  $\tau$  is computed assuming that is equal to both tensile and compression principal stresses, as follows:

$$\tau = \frac{P \cos \theta}{A_n} \quad (2)$$

where  $\theta$  is the angle between the horizontal and the main diagonal of the wall,  $A_n$  is the net area of the masonry specimen calculated as:



$$A_n = \left(\frac{W+H}{2}\right) Tn \quad (3)$$

318

319 with  $W$ ,  $H$ , and  $T$  the width, height, and thickness of the specimen, respectively, and  $n$  is the percentage of the  
 320 gross area of the unit that is solid, expressed as a decimal [52]. In this study, the value of  $n$  is equal to 1. The  
 321 shear strain  $\gamma$  is calculated as:

322

$$\gamma = \frac{\Delta v + \Delta u}{g} \quad (4)$$

324

325 where  $\Delta v$  is the average vertical shortening (in mm) measured by the horizontal LVDTs,  $\Delta u$  is the average  
 326 horizontal extension (in mm) measured by the vertical LVDTs, Fig. 5, and  $g$  is the vertical gage length (in  
 327 mm), which in this study is 500 mm.

328 Referring to shear stress–strain curves for the URM specimens displayed in Fig. 6a, an approximately linear  
 329 behavior until the end of the test can be identified. As soon as the crack appeared at the brick/mortar interface  
 330 and the peak stress was reached, specimens collapsed in a brittle way. It should be noted that results related to  
 331 specimen URM-3 are not reported due to an anomalous behaviour of the wallette during the testing procedure.  
 332 The shear stress–strain curves for specimens strengthened by NSM bars are represented in Fig. 6b, as well as  
 333 the curves for the URM specimens for comparison purposes. Curves for the RR-A specimens show a similar  
 334 slope in the initial part. On average, the maximum shear stress is similar between asymmetrically reinforced  
 335 specimens and URM walls, whereas displacement capacity is higher. Wallettes with twice the amount of  
 336 reinforcement (RR-S) behave in a linear elastic manner at low load values, then a non-linear behavior is  
 337 observed till the peak load. Initial cracking is delayed by the presence of the reinforcement and the shear  
 338 modulus increases with the presence of the bars. RR-S-1 wallette shows an anomalous behaviour in the initial  
 339 part characterized by a low rigidity: a possible reason of this behaviour can be related to the strengthening  
 340 operations and it will be discussed in the next section.

341 Curves for RF-A and RF-S specimens are shown in Fig. 6c. Results are less dispersed with respect to RR  
 342 specimens and a clear and consistent trend can be envisaged. The curves are steeper in the first part with a  
 343 substantial increase for the shear modulus with respect to URM curves. As expected, the highest peak stresses  
 344 are reached by the specimens reinforced symmetrically (RF-S). However, a remarkable increment in peak  
 345 stress is also registered for specimens reinforced on only one side (RF-A). FRCM composite applied on the  
 346 face of the specimens restrained the opening of diagonal cracks allowing the wallettes to undergo larger  
 347 displacements (shear strain higher than 1 cm/m) and substantially increased the shear stiffness of the masonry  
 348 specimens.

349

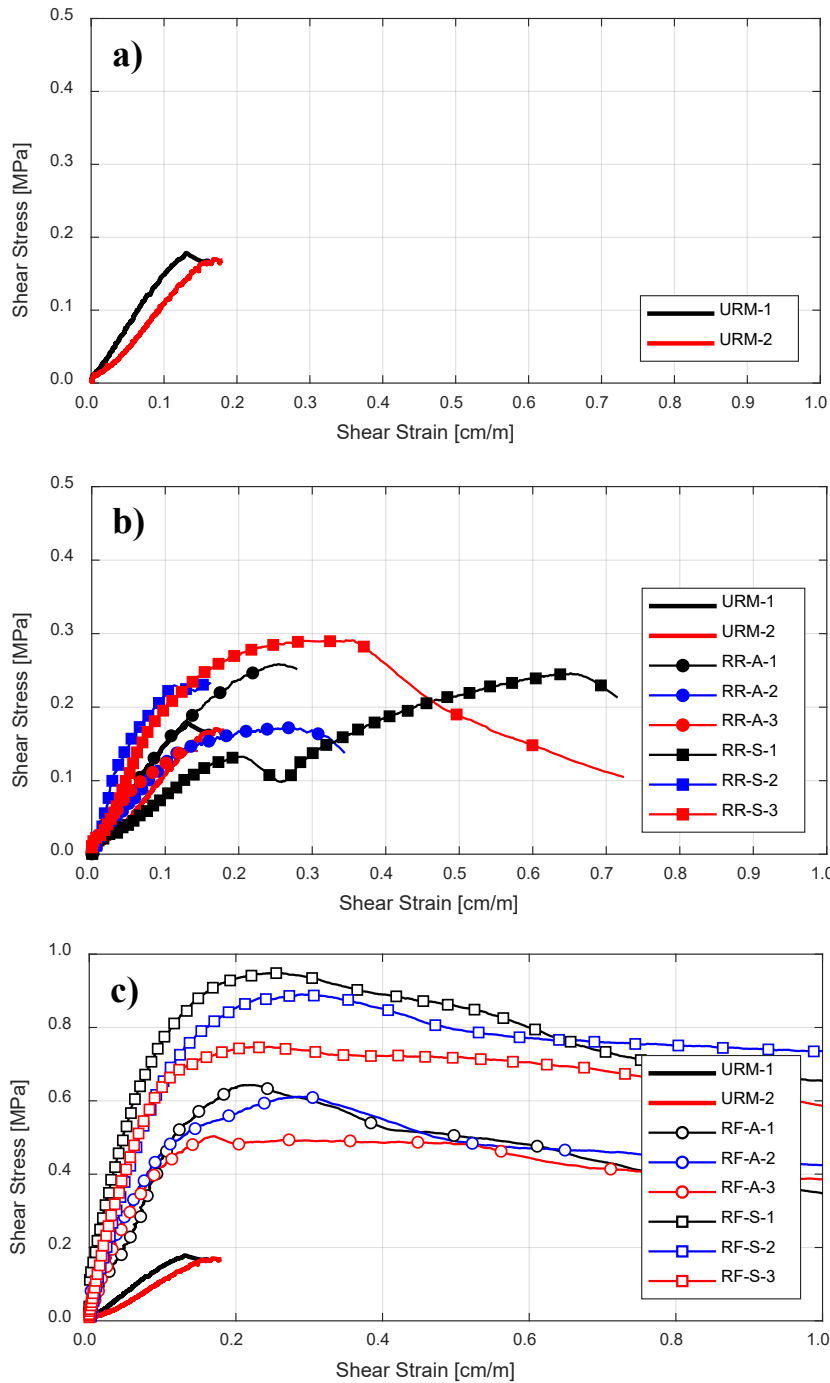


Fig. 6. Shear stress-strain curves for the tested specimens: a) URM specimens; b) strengthened specimens by using NSM bars; c) strengthened specimens by using FRCM system.

#### 4.2. Crack pattern and failure mode

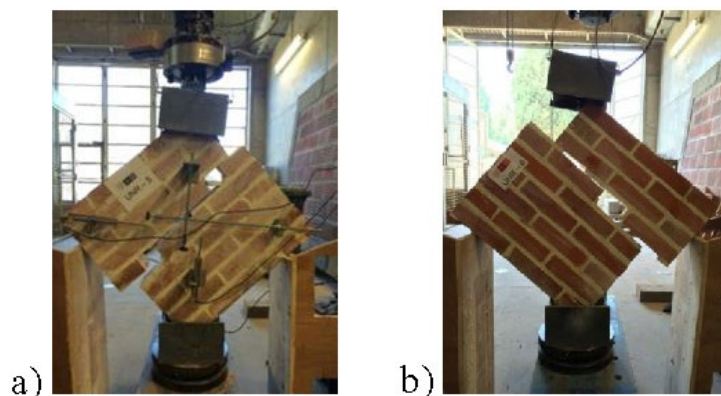
It was observed that URM specimens collapsed in a brittle way, in which a main crack developed within the mortar joints, and sliding occurred due to detachment at the brick/mortar interface: bonding between the masonry units and mortar controlled the failure, as shown in Fig. 7a and Fig. 7b.

In the case of RR-A and RR-S wallettes, the presence of the bars did not change the failure mode with respect to URM specimens, which still was sliding along the unreinforced mortar joints, see Fig. 8a - Fig. 8f. In some

362 repointed specimens, failure occurred due to sliding at the brick/mortar interface partially involving the  
 363 strengthened joints (e.g. RR-A-2 and RR-A-3 specimens). Specimen RR-S-1, symmetrically repointed, as  
 364 already noted in the previous section, showed an anomalous behaviour: the crack that led to the collapse of the  
 365 specimen propagated from the upper reinforced joint, see Fig. 8d. This behaviour may be attributed to the  
 366 repointing operations, as the slots in the joints were made with a grinder after the curing of the panels. This  
 367 procedure may have caused an initial damage in the joint, creating a weak plane, which led consequently to  
 368 the collapse of the specimen involving that joint. It is believed that this effect would be less relevant for thicker  
 369 wallettes, which is the case of real buildings. Additionally, in specimens RR-A-2, RR-A-3 and RR-S-1  
 370 debonding of the bar from the surrounding mortar was visible, Fig. 8d. This behaviour usually is not detected  
 371 in the case of NSM bars embedded with epoxy resin [29], where the epoxy paste and the bar do not detach one  
 372 with respect to the other, while the bond at the paste/masonry interface controls failure. In the development of  
 373 the analytical approach presented in Section 5.2, this aspect will be taken into account.

374 Referring to the failure mode of RF-A specimens, Fig. 9a - Fig. 9c, once the peak load was attained, vertical  
 375 cracks started to appear in the central area, clearly visible on the specimen side not covered by the FRCM  
 376 composite, involving both the joints and the bricks, see Fig. 9a. As the cracking pattern developed and the  
 377 cracks got wider, the specimen started to tilt towards the reinforced side as already noted in other experimental  
 378 campaigns [29]. This behavior was neither detected in the symmetrically FRCM reinforced panels nor in the  
 379 case of NSM reinforced panels. This out-of-plane effect did not result in a ductility reduction. Cracks kept  
 380 evolving along the compressed diagonal, between the two loading shoes, leaving the outer corners unaffected.  
 381 Finally, FRCM debonded from the masonry and the specimens failed due to diagonal tension.

382 Failure mode of RF-S specimens, Fig. 9d - Fig. 9f, was characterized by vertical cracks that appeared in the  
 383 mid part of the specimen body. The cracking pattern developed within the two loading shoes, and a diagonal  
 384 tension failure occurred in the specimens. At failure, the FRCM layers debonded from the masonry on both  
 385 sides. It is thus believed that the use of anchorage systems may further increase the load and displacement  
 386 capacities, but this topic is outside the scope of the present study. A summary of the cracking patterns of the  
 387 retrofitted walls is given in Fig. 10.



389  
 390 Fig. 7. Failure mode of unreinforced specimens: a) UMR-1; b) URM-2.

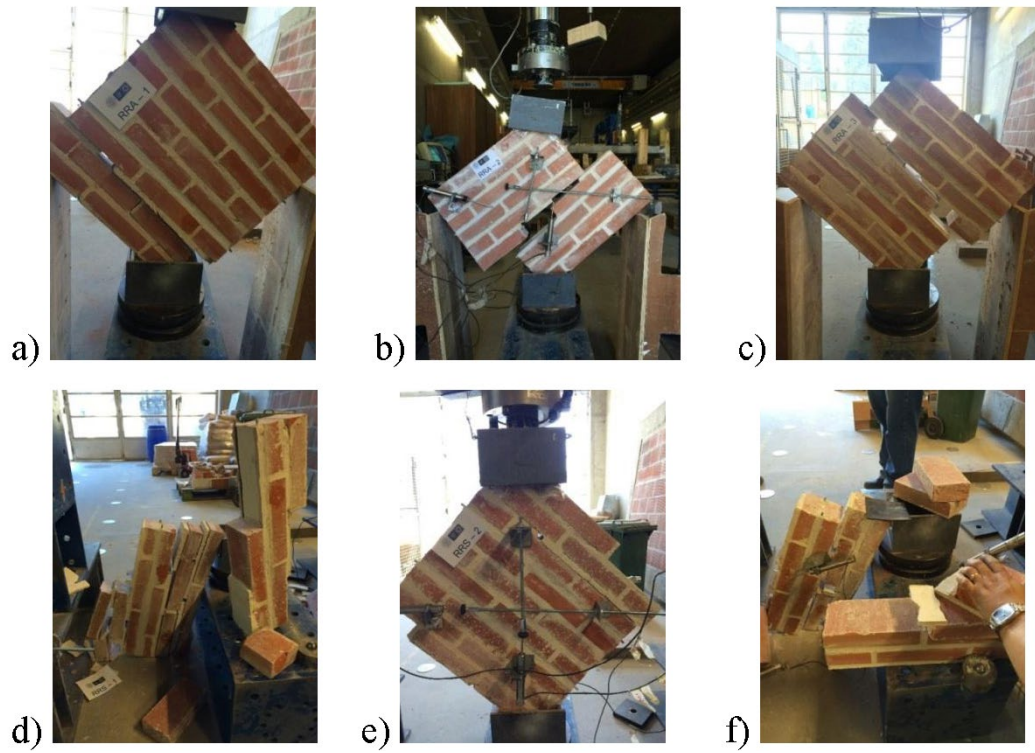


Fig. 8. Failure mode of RR specimens: a) RR-A-1, b) RR-A-2, c) RR-A-3, d) RR-S-1, e) RR-S-2 and f) RR-S-3.

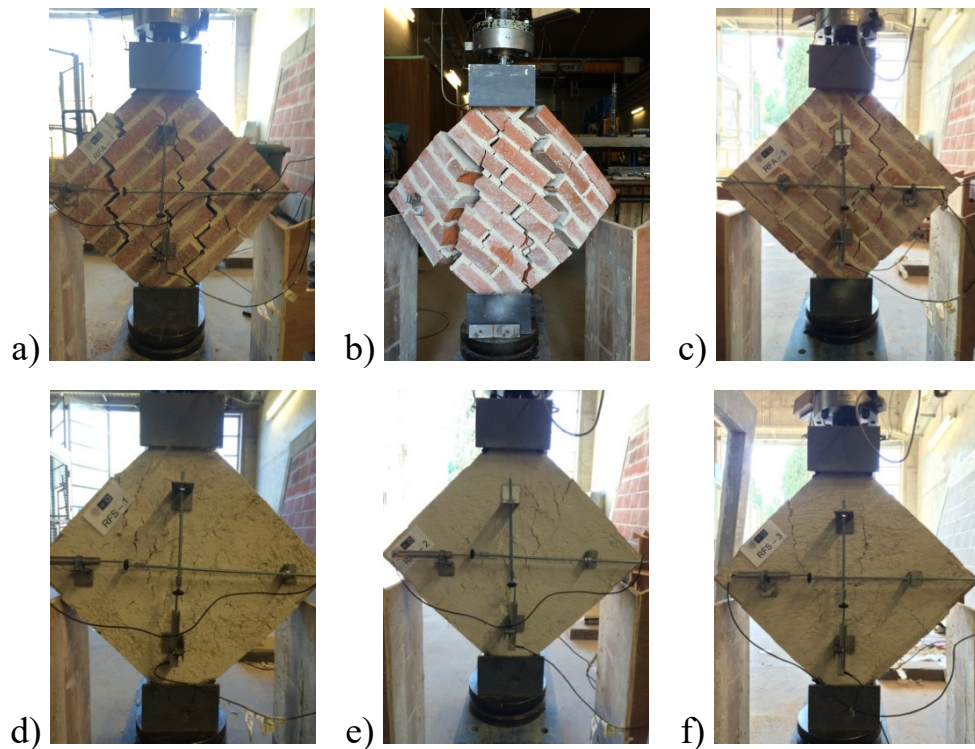


Fig. 9. Failure mode of RF specimens: a) RF-A-1, b) RF-A-2, c) RF-A-3, d) RF-S-1, e) RF-S-2 and f) RF-S-3.

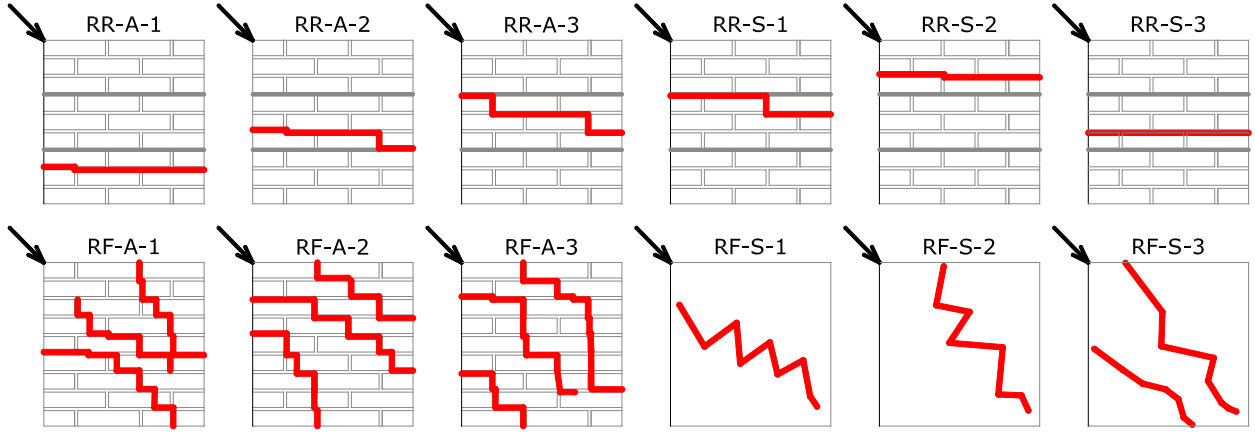


Fig. 10. Cracking patterns of the retrofitted wallets.

#### 4.3. Summary results

A summary of the relevant mechanical parameters obtained from the diagonal compression tests in terms of average values and coefficients of variation is given in Table 4. The peak load and shear stress values ( $P_{max}$ ,  $\tau_{max}$ ) are also listed. The strength enhancement in terms of maximum force,  $\Delta$ , achieved by using reinforcements, is calculated as follows:

$$\Delta = \left( \frac{\bar{P}_{max}^R - \bar{P}_{max}^{URM}}{\bar{P}_{max}^{URM}} \right) 100\% \quad (5)$$

where  $\bar{P}_{max}^R$  and  $\bar{P}_{max}^{URM}$  are the average peak forces for the reinforced specimens (RR-A, RR-S, RF-A and RF-S) and unreinforced specimens (URM), respectively. The elastic shear modulus is derived as:

$$G = \frac{\tau_{el}}{\gamma_{el}} \quad (6)$$

where  $\tau_{el}$  is the shear stress in the elastic branch and  $\gamma_{el}$  is the corresponding shear strain. The displacement ductility of the considered retrofitting solutions,  $\mu$ , is here evaluated as:

$$\mu = \min \left( \frac{\Delta u_u}{\Delta u_{max}}; \frac{\Delta v_u}{\Delta v_{max}} \right) \quad (7)$$

where  $\Delta u_u$  and  $\Delta v_u$  are the horizontal elongation and vertical shortening corresponding to the ultimate conditions, respectively, while  $\Delta u_{max}$  and  $\Delta v_{max}$  are the horizontal elongation and vertical shortening corresponding to the maximum load, respectively. In particular, in the case of repointing strengthening, the ultimate displacements are taken at failure, whereas for the FRCM strengthening, the ultimate condition is considered to occur when the post-peak load reaches the 80% of its maximum value, as in [10, 36, 53]. A masonry panel that experiences inelastic deformations without substantial load-carrying capacity reduction is characterized by a high value of  $\mu$ .

423 Finally, in order to compare the two retrofitting solutions, the parameter  $\rho_f$ , Eq. (1), representing the calibrated  
 424 reinforcement ratio, is reported as well.

425 From Table 4, by comparing the results for URM and RR-A specimens in terms of peak load, the increment  $\Delta$   
 426 reaches 8%, whereas for RR-S specimens it attains 44%. Moreover, an increment in the shear modulus,  
 427  $\bar{G}$ , moving from URM specimens to RR is registered. In terms of ductility, it is worth noting that  $\mu$  is lower  
 428 for RR-S with respect to RR-A. As stated before, an induced initial damage may have been caused during the  
 429 strengthening operation. Additionally, also due to the brittle failure of the specimens, the values of  
 430 displacements at ultimate conditions employed to calculate the ductility value, Eq. (7), were not easy to  
 431 identify.

432 Comparing the results for URM and RF-A specimens in terms of  $\bar{P}_{max}$ , the increment is double, whereas  
 433 between URM and RF-S, the increment is three times higher. An increment in shear modulus,  $\bar{G}$ , is achieved  
 434 moving from URM to RF specimens. The ductility  $\mu$  is twice when compared to the one obtained for the  
 435 reinforced specimens with the repointing technique. In fact, the presence of the FRCM reinforcement modifies  
 436 the mode of failure from sliding (URM and RR specimens) to diagonal tension (RF specimens). Application  
 437 of the FRCM only on one side of the panel leads to a substantial increment in the load capacity and pseudo-  
 438 ductility value, and this increment is even more marked for the symmetric retrofitting solution.

439

440 Table 4. Summary of the main experimental results (the coefficient of variation is given inside parentheses).

Specimen label	$P_{max}$ [kN]	$\bar{P}_{max}$ [kN]	$\tau_{max}$ [MPa]	$\bar{\tau}_{max}$ [MPa]	$\Delta$ [%]	$G$ [MPa]	$\bar{G}$ [MPa]	$\mu$ [/]	$\bar{\mu}$ [/]	$\rho_f$ [%]
URM-1	12.99	13.32	0.17	0.18	-	141.03	173.09 (26%)	-	-	-
URM-2	13.65	(4%)	0.18			205.15				
RR-A-1	11.07	14.62 (30%)	0.15	0.20	8.0	297.60	253.02 (32%)	-	1.21 (8%)	0.46
RR-A-2	13.18		0.18			159.90		1.28		
RR-A-3	19.60		0.26			301.58		1.14		
RR-S-1	18.65	19.48 (12%)	0.25	0.26	44.0	155.21	403.92 (54%)	1.18	1.09 (8%)	0.92
RR-S-2	17.71		0.24			559.56		1.00		
RR-S-3	22.09		0.30			497.00		1.08		
RF-A-1	45.83	43.96 (12%)	0.62	0.59	224.8	773.09	672.78 (17%)	1.57	2.09 (44%)	0.75
RF-A-2	48.11		0.65			693.37		1.55		
RF-A-3	37.95		0.51			551.88		3.14		
RF-S-1	66.61	64.45 (12%)	0.90	0.87	376.2	1696.50	2050.25 (35%)	2.79	2.82 (21%)	1.50
RF-S-2	70.91		0.95			2881.46		2.24		

RF-S-3	55.84		0.75			1572.80		3.44		
--------	-------	--	------	--	--	---------	--	------	--	--

Furthermore, it can be noted that even if the reinforcement ratio is not negligible in the case of repointed panels, the corresponding load carrying capacity increment with respect to the control specimens is not so substantial. As expected, the FRCM symmetric and asymmetric application lead to a peak increment and pseudo-ductility increment that are higher. As already noted in other experimental campaigns [33, 35], an increment of the reinforcement ratio does not always lead to a proportional increment in shear capacity and ductility. However, in the cases where EB textiles cannot be applied in façades of masonry structures or monuments due to preservation criteria, it is shown that structural repointing provides additional resources of ductility and energy absorption capacity to masonry.

The most remarkable change highlighted in the specimens retrofitted with the bars with respect to URM panels is the increment in displacement capacity. As expected, a more evident structural enhancement in the wall panels is registered using the FRCM system, resulting in a clear increment of both shear strength and displacement capacity.

## 5. Analytical investigation

The analytical procedure presented in ACI 549 [30] to predict the nominal shear capacity of unreinforced masonry walls is followed in this section and analytical results are compared with the corresponding experimental ones.

Considering a reinforced masonry panel subjected to a diagonal compression load  $P$ , the nominal shear capacity of the panel,  $V_n$ , can be computed as the sum of two contributions:

$$V_n = V_m + V_f \quad (8)$$

where  $V_m$  and  $V_f$  are the contributions of the masonry panel and the reinforcement, respectively.

### 5.1. URM specimens

In a diagonal compression test, four types of failure mechanisms are identified, depending on physical and mechanical properties of the wall [29, 31]. The specimen fails when the shear load reaches the minimum shear capacity,  $V_m$ , as follows:

$$V_m = \min\{V_{SS}, V_{Sf}, V_{dt}, V_c\} \quad (9)$$

The shear capacity due to shear sliding failure,  $V_{SS}$ , is given by:

$$V_{SS} = \frac{\tau_0}{1 - \mu_0 \tan \theta} A_n \quad (10)$$



476

477 where  $\tau_0$  is the shear bond strength between mortar and bricks,  $\mu_0$  is the coefficient of internal shear friction  
 478 in mortar joints, and  $A_n$  is calculated by using Eq. (3). Parameters  $\tau_0$  and  $\mu_0$  can be experimentally determined  
 479 by means of the triplet test, as described in [54].

480 The shear capacity due to shear friction failure,  $V_{sf}$ , is equal to:

481

$$482 \quad V_{sf} = \frac{\tau_{0,m}}{1 - \mu_m \tan \theta} A_n \quad (11)$$

483

484 where  $\tau_{0,m}$  and  $\mu_m$  are the modified shear bond strength in the mortar joints and the modified coefficient of  
 485 internal shear friction in the mortar joints, respectively, calculated as

486

$$487 \quad \tau_{0,m} = \frac{\tau_0}{1 + 1.5 \mu_0 \frac{h}{w}} \quad (12)$$

488

489 and

490

$$491 \quad \mu_m = \frac{\mu_0}{1 + 1.5 \mu_0 \frac{h}{w}} \quad (13)$$

492

493 with  $w$  and  $h$  being the width and height of the brick, respectively.

494 The shear capacity due to the diagonal tension failure,  $V_{dt}$ , results in:

495

$$496 \quad V_{dt} = \frac{\tan \theta + \sqrt{21.26 + \tan^2 \theta}}{10.58} f'_t A_n \quad (14)$$

497

498 where the tensile strength of masonry  $f'_t$  is considered equal to  $0.67\sqrt{f'_m}$  for clay bricks, with  $f'_m$  being the  
 499 compressive strength of masonry.

500 Finally, the shear capacity due to toe crushing failure at the loaded end,  $V_c$  is given by:

501

$$502 \quad V_c = \frac{2wf'_m}{3h + 2w \tan \theta} A_m \quad (15)$$

503

504 where  $A_m$  is the interface loading area between the steel shoe and the wall along the horizontal direction [31].

505

## 506 5.2. RR-A and RR-S specimens: NSM bar contribution

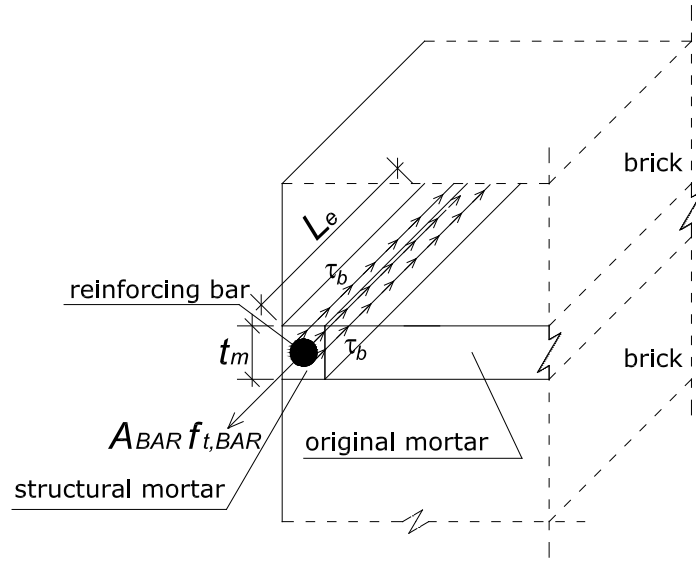
507 In order to calculate the  $V_f$  contribution given by the basalt bars, a modified version of the approach presented  
 508 by [29] is followed here. In [29], diagonal compression tests on unreinforced masonry concrete walls  
 509 strengthened with glass fiber-reinforced polymer bars were presented. The glass bars were embedded in the



510 mortar joints by means of an epoxy paste and a latex modified cementitious paste. In all the tests, neither  
 511 debonding of FRP bars from the paste nor tensile failure of the bars were observed. Thus, in calculating the  
 512 contribution of the FRP bars to the shear capacity of the walls, a perfect bond between the bar and the epoxy  
 513 paste was considered. As a consequence, the shear resistance of the reinforcing bars was limited by bond failure  
 514 between epoxy paste and the surrounding original mortar.

515 In the present study, after the failure of the walls reinforced by means of repointing, it was observed that the  
 516 basalt bars were in some parts detached from the surrounding structural mortar. For this reason, the approach  
 517 in [29] was modified taking into account that the shear resistance of the basalt bars is controlled by bond failure  
 518 between the structural mortar and the bar itself.

519



520

521 Fig. 11. Distribution of the stresses along a bar embedded in the mortar joint.

522

523 In the analysis, the bond stress between structural mortar and the bar is assumed to be uniform along the  
 524 effective length of the bar at failure, Fig. 11. From equilibrium conditions, the tensile force developed in the  
 525 bar should be equal to the bond strength between the structural mortar and the bar:

526

$$527 \quad \tau_b A_b = f_{t, BAR} A_{BAR} \quad (16)$$

528

529 where  $\tau_b$  and  $A_b$  are the average bond strength and average bond area between the bar and the structural mortar,  
 530  $f_{t, BAR}$  is the tensile stress of the NSM bar and  $A_{BAR}$  is the cross-sectional area of the bar. The average bond  
 531 area  $A_b$  is equal to

532

$$533 \quad A_b = 2\pi R_{BAR} L_e \quad (17)$$

534

535 where  $R_{BAR}$  is the nominal radius of the bar and  $L_e$  is the effective length of the bar in masonry.

536 Substituting Eq. (17) in Eq. (16), the effective length results

537

$$538 \quad L_e = \frac{f_{t,BAR} R_{BAR}}{2\tau_b} \quad (18)$$

539

540 Following [29], it is assumed that: *i*) in the masonry wall during the diagonal test, a shear crack with a constant  
 541 inclination angle of 45 degrees is considered; *ii*) each bar intersected by the crack is divided into two parts at  
 542 the two sides of the crack. The shear resistance provided by the bars,  $V_f$ , is computed as the sum of the forces  
 543 resisted by the bars intersecting the diagonal crack. The force carried by each bar is calculated as the product  
 544 of the average bond strength and the surface area of the bond between bar and structural mortar according to  
 545 the effective bond length of the bar, which is the shortest part of the bar intersected by the diagonal crack.  
 546 Therefore,  $V_f$  reads

547

$$548 \quad V_f = \sum_{i=1}^N A_{BARi} f_i = \tau_b 2\pi R_{BAR} \sum_{i=1}^n L_i \quad L_i \leq L_e \quad (19)$$

549

550 where  $f_i$  is the force carried by  $i$ -th reinforcing bar,  $N$  is the total number of bars intersected by the diagonal  
 551 crack and  $L_i$  is the effective bond length of the  $i$ -th bar intersecting the diagonal crack.

552

### 553 5.3. RF-A and RF-S specimens: FRCM contribution

554 The contribution of FRCM composite to the shear capacity,  $V_f$ , is calculated following [31] as:

555

$$556 \quad V_f = 2n_{layer} A_{FRCM} W f_{t,FRCM} \quad (20)$$

557

558 where  $n_{layer}$  is the number of layers of fabric,  $A_{FRCM}$  is the area of fabric reinforcement by unit width in both  
 559 horizontal and vertical directions,  $f_{t,FRCM}$  is the tensile strength in the FRCM reinforcement calculated as:

560

$$561 \quad f_{t,FRCM} = E_{FRCM} \varepsilon_u \quad (21)$$

562

563 where  $E_{FRCM}$  and  $\varepsilon_u$  are the tensile modulus of elasticity of the cracked FRCM and the tensile strain in the  
 564 FRCM reinforcement, respectively. Parameter  $\varepsilon_u$  coincides with the ultimate tensile strain  $\varepsilon_{FRCM}$  if the latter  
 565 value is smaller than 0.004 according to [30]. All the calculations to determine the shear capacities of the  
 566 unreinforced and reinforced wallettes tested in this research program are given in Appendix A.

567

### 568 5.4. Summary results

569 A comparison between the experimental and the analytical results in terms of shear capacity is listed in Table  
 570 5. The contribution of the reinforcement separated from the contribution to the shear capacity of URM panels  
 571 is reported as well. It can be observed that the strength of the unreinforced panels is not accurately predicted,  
 572 since the ratio between experimental and analytical result is 0.77. This may be due to the fact that the shear

friction capacity found analytically assumes at failure a stepped crack through the diagonal wall, while in the case of the two walls tested in this experimental campaign, the crack pattern involved a smaller surface. For specimens reinforced on one or both sides with repointing technique, analytical results overestimate the strength, while for the case of FRCM composites, the formula from [30] provides a large safety margin against the results obtained experimentally. Isolating the contribution of the reinforcement, it can be noted that in the case of asymmetric repointing the contribution of the bars is overestimated from the analytical approach, while the ratio between the experimental and analytical value is around one in the case of symmetric configuration of strengthening. In the case of FRCM, the contribution of the composite found experimentally is almost three times higher than the one determined analytically. The discrepancies between experimental and analytical values in the case of NSM reinforcement can be ascribed to different factors. The analytical procedure employed to calculate the enhancement of shear capacity given by NSM bars is based on several hypotheses. The procedure is an adaptation of the method employed for NSM bars embedded with epoxy paste in masonry joints: the failure mode between the two compared systems (grout-based and epoxy-based) is different, since in the case of grout-filled grooves, failure is controlled by the bond between the grout and the bar, differently from the case of epoxy-filled grooves where the governing factor is the bond between the epoxy paste and the substrate material. Further, in the analytical approach a uniform distribution of the shear stress along the embedment length of the bars is considered. The analytical model employed to calculate the contribution of the bar reinforcement requires further improvements and additional validations considering data from other experimental campaigns.

Table 5. Comparison between experimental and analytical results in terms of shear capacity.

	Strength (exp.)	Strength (ana.)	Ratio (exp./ana.)	Contribution of the reinforcement (exp.)	Contribution of the reinforcement (ana.)	Ratio considering only the contribution of the reinforcement (exp./ana.)
URM [kN]	9.42	12.15	0.77	/	/	/
RR-A [kN]	10.34	14.27	0.72	0.92	2.12	0.43
RR-S [kN]	13.77	16.39	0.84	4.35	4.24	1.03
RF-A [kN]	31.08	18.09	1.72	21.66	5.94	3.64
RF-S [kN]	45.57	24.03	1.90	36.15	11.88	3.04

## 6. Conclusions

An experimental campaign on diagonal compression tests conducted on clay brick masonry panels strengthened by two different techniques was presented in this paper. In particular, the investigated strengthening systems were: (a) structural repointing by inserting basalt bars in the mortar joints in a symmetric and asymmetric configuration; (b) FRCM composites by applying a glass mesh on one or both sides of the specimens.

Diagonal compression tests allowed to investigate the shear load capacity as well as the ductility of the tested

specimens. In particular, an increase in maximum load, shear stiffness and ductility was registered for both retrofitting solutions. However, the increment in shear capacity and ductility is not proportional to the reinforcement ratio, highlighting that an increment of reinforcement does not necessarily correspond to a better structural performance, as pointed out in literature. The failure mode in the case of repointing was sliding along the interface between bricks and mortar as observed in URM specimens, while in the case of FRCM strengthened panels, the mode of failure was diagonal cracking. In the case of asymmetric FRCM reinforcement, the panels bent towards the reinforced side.

Analytical procedures showed to be effective in predicting conservative values of shear capacities of reinforced specimens with FRCM. However, some built-in variabilities of URM and repointed panels justify differences between theoretical and experimental results. Additionally, it should be considered that analytical results depend on the values chosen for the parameters, thus for a more reliable prediction of the shear strength, it is recommended that the required parameters are derived by means of experimental tests on the same materials adopted in the program.

## Acknowledgments

This work was partly financed by FEDER funds through the Operational Programme Competitiveness Factors (COMPETE) and by national funds through the Foundation for Science and Technology (project POCI-01-0145-FEDER-007633). The collaboration of Mr. Mattia Girolomini and the support of the technical staff from the Structural Laboratory of University of Minho during the experimental campaign are gratefully acknowledged. Authors are also grateful to MagmaTech Ltd for kindly providing the basalt bars.

## Appendix A

### A.1 Masonry properties

Width of the brick:  $w = 200$  mm

Height of the brick:  $h = 50$  mm

Thickness of the brick  $t = 100$  mm

Width of the specimen:  $W = 520$  mm

Height of the specimen:  $H = 530$  mm

Thickness of the specimen:  $T = 100$  mm

Thickness of the mortar joint:  $t_m = 10$  mm

Net area of the specimen:  $A_n = 52500$  mm<sup>2</sup>

Compressive strength of brick:  $f_{cb} = 14.3$  MPa

Compressive strength of mortar A:  $f_{cm} = 5.8$  MPa

Compressive strength of masonry:  $f'_m = K f_{cb}^{0.7} f_{cm}^{0.3} = 0.55 \cdot 14.3^{0.7} \cdot 5.8^{0.3} = 6.00$  MPa (according to EN 1996-1-1 [55] assuming masonry made by general purpose mortar)

Tensile strength of masonry:  $f'_t = 0.67 \sqrt{f'_m} = 1.64$  MPa

Elastic modulus of masonry:  $E_m = 1000 f'_m = 6000$  MPa (from [56])

639 Shear bond strength of mortar joint:  $\tau_0 = 3\% f'_m = 0.180$  MPa (from [31])  
640 Coefficient of internal shear friction in mortar joints:  $\mu_0 = 0.30$  (from [31, 57])  
641 Modified shear bond strength of mortar joint:  $\tau_{0,m} = 0.169$  MPa  
642 Modified coefficient of internal shear friction in mortar joints:  $\mu_m = 0.270$   
643 Average bond strength between the bar and the structural mortar:  $\tau_b = 0.5$  MPa (in [29],  $\tau_b$  is assumed equal  
644 to 1.74 MPa. However, this value is referred to triplet tests performed on masonry made by concrete blocks  
645 and joints made by epoxy paste. In this study, no triplets tests were conducted to identify the average bond  
646 strength between the bar and the mortar, as a consequence the value  $\tau_b$  is taken from literature on similar  
647 materials [58, 59]).

#### 649 *A.2 Basalt bar properties*

650 Diameter of the bar:  $\phi_{BAR} = 5.5$  mm  
651 Cross-sectional area of the bar:  $A_{BAR} = 23.76$  mm<sup>2</sup>  
652 Elastic modulus of the bar:  $E_{BAR} = 34182$  MPa  
653 Maximum tensile strength of the bar:  $f_{t,BAR} = 777.27$  MPa

#### 655 *A.3 FRCC properties*

656 Area of FRCC reinforcement by unit width in both directions:  $A_{FRCC} = 35.27$  mm<sup>2</sup>/m  
657 Elastic modulus of FRCC (cracked):  $E_{FRCC} = 40500$  MPa

#### 659 *A.4 Masonry contribution ( $V_m$ )*

660 (a) Shear capacity due to shear sliding failure,  $V_{SS}$ :

$$661 \quad V_{SS} = \frac{\tau_0}{1 - \mu_0 \tan \theta} A_n = \frac{0.180}{1 - 0.30 \cdot 1} 52500 = 13500 \text{ N} = 13.5 \text{ kN}$$

662 (b) Shear capacity due to shear friction failure,  $V_{Sf}$ :

$$663 \quad V_{Sf} = \frac{\tau_{0,m}}{1 - \mu_m \tan \theta} A_n = \frac{0.169}{1 - 0.270 \cdot 1} 52500 = 12154 \text{ N} = 12.15 \text{ kN}$$

664 (c) Shear capacity due to the diagonal tension failure,  $V_{dt}$ :

$$665 \quad V_{dt} = \frac{\tan \theta + \sqrt{21.26 + \tan^2 \theta}}{10.58} f'_t A_n = \frac{1 + \sqrt{21.26 + 1}}{10.58} 1.64 \cdot 52500 = 46533 \text{ N} = 46.53 \text{ kN}$$

666 (d) Shear capacity due to toe crushing failure at the loading end,  $V_c$ :

$$667 \quad V_c = \frac{2w f'_m}{3h + 2w \tan \theta} A_m = \frac{2 \cdot 200 \cdot 6.00}{3 \cdot 50 + 2 \cdot 200 \cdot 1} \cdot 100 \cdot 100 = 43636 \text{ N} = 43.64 \text{ kN}$$

668 Finally, URM shear capacity is calculated by using Eq. (8) as:

$$669 \quad V_m = \min\{V_{SS}, V_{Sf}, V_{dt}, V_c\} = \min\{13.5, 12.15, 46.53, 43.64\} \text{ kN} = 12.15 \text{ kN}$$

#### 671 *A.5 Bars contribution ( $V_f$ )*

$$L_e = \frac{f_{t,BAR} R_{BAR}}{2\tau_b} = \frac{777.27 \text{ MPa} \cdot 2.25 \text{ mm}}{2 \cdot 0.5 \text{ MPa}} = 2137.49 \text{ mm} = 2.1 \text{ m}$$

$$V_f = \tau_b 2\pi R_{BAR} \sum_{i=1}^n L_i \quad L_i \leq L_e$$

$$\text{asymmetric reinforcement: } V_f = 0.5 \text{ MPa} \cdot 2 \cdot \pi \cdot 2.25 \text{ mm} \cdot (200 + 100) \text{ mm} = 2.12 \text{ kN}$$

$$\text{symmetric reinforcement: } V_f = 0.5 \text{ MPa} \cdot 2 \cdot \pi \cdot 2.25 \text{ mm} \cdot (200 \cdot 2 + 100 \cdot 2) \text{ mm} = 4.24 \text{ kN}$$

676

#### 677 *A.6 FRCM contribution ( $V_f$ )*

678 From technical data, the ultimate tensile strain  $\varepsilon_u$  of FRCM is equal to 0.0098, thus higher than 0.004 that  
679 represents the admissible value according to ACI 549 [30]. As a consequence,  $\varepsilon_u$  is considered equal to 0.004.

$$680 \quad f_{t,FRCM} = E_{FRCM} \varepsilon_u = 40500 \cdot 0.004 = 162 \text{ MPa}$$

$$681 \quad V_f = 2n_{layer} A_{FRCM} W f_{t,FRCM}$$

$$682 \quad \text{asymmetric reinforcement: } V_f = 2 \cdot 1 \cdot 35.27 \text{ mm}^2 / 1000 \text{ mm} \cdot 520 \text{ mm} \cdot 162 \text{ N/mm}^2 = 5942.3 \text{ N} =$$

$$683 \quad 5.94 \text{ kN}$$

$$684 \quad \text{symmetric reinforcement: } V_f = 2 \cdot 2 \cdot \frac{35.27 \text{ mm}^2}{1000 \text{ mm}} \cdot 520 \text{ mm} \cdot \frac{162 \text{ N}}{\text{mm}^2} = 11884.6 \text{ N} = 11.88 \text{ kN}$$

685

#### 686 *A.6.1 Limitations*

687 Following ACI 549 [30], the summation of the masonry and FRCM shear contributions should be checked  
688 against the substrate toe crushing capacity:

$$689 \quad V_n = \min(V_m + V_f; V_c) = \min(12.15 + 5.94; 43.64) = 18.09 \text{ kN}$$

690

#### 691 **References**

- 692 [1] Boscato, G., Pizzolato, M., Russo, S. (2014) ‘Seismic behavior of a complex historical church in l’Aquila’,  
693 *International Journal of Architectural Heritage*, Vol. 8, pp. 718-757.
- 694 [2] Franzoni, E., Gentilini, C., Graziani, G., Bandini, S. (2015) ‘Compressive behaviour of brick masonry  
695 triplets in wet and dry conditions’, *Construction and Building Materials*, Vol. 82, pp. 45-52.
- 696 [3] Xu, H., Gentilini, C., Yu, Z., Wu, H., Zhao, S. (2018) ‘A unified model for the seismic analysis of brick  
697 masonry structures’, *Construction and Building Materials*, Vol. 184, pp. 733-751.
- 698 [4] Viskovic, A. (2016) ‘Seismic retrofitting for masonry historical buildings: Design philosophy and hierarchy  
699 of interventions’, *Civil and Environmental Engineering: Concepts, Methodologies, Tools, and*  
700 *Applications*, Vol. 1, pp. 480-503 (Book Chapter).
- 701 [5] Maddaloni, G., Di Ludovico, M., Balsamo, A., Maddaloni, G., Prota, A. (2018) ‘Dynamic assessment of  
702 innovative retrofit techniques for masonry buildings’, *Composites Part B: Engineering*, Vol. 147, pp.  
703 147-161.
- 704 [6] Vaculik, J., Visintin, P., Burton, N.G., Griffith, M.C., Seracino, R. (2018) ‘State-of-the-art review and  
705 future research directions for FRP-to-masonry bond research: Test methods and techniques for

- 706 extraction of bond-slip behavior', *Construction and Building Materials*, Vol. 183, pp. 325-345.
- 707 [7] Foraboschi, P. (2016) Effectiveness of novel methods to increase the FRP-masonry bond capacity,  
708 *Composites Part B: Engineering*, Vol. 107, pp. 214-232.
- 709 [8] Valluzzi, M. R., Tinazzi, D., Modena, C. (2002) 'Shear behavior of masonry panels strengthened by FRP  
710 laminates', *Construction and Building Materials*, Vol. 16, pp. 409-416.
- 711 [9] Babatunde, S.A. (2017) 'Review of strengthening techniques for masonry using fiber reinforced polymers',  
712 *Composite Structures*, Vol. 161, pp. 246-255.
- 713 [10] Gattesco, N., Boem, I. (2015) 'Experimental and analytical study to evaluate the effectiveness of an in-  
714 plane reinforcement for masonry walls using GFRP meshes', *Construction and Building Materials*,  
715 Vol. 88, pp. 94-104.
- 716 [11] Marcari, G., Basili, M., Vestroni, F. (2017) 'Experimental investigation of tuff masonry panels reinforced  
717 with surface bonded basalt textile-reinforced mortar', *Composites Part B: Engineering*, Vol. 108, pp.  
718 131-142.
- 719 [12] Cevallos, O.A., Olivito, R.S., Codispoti, R., Ombres, L. (2015) 'Flax and polyparaphenylene  
720 benzobisoxazole cementitious composites for the strengthening of masonry elements subjected to  
721 eccentric loading', *Composites Part B: Engineering*, Vol. 71, pp. 82-95.
- 722 [13] Franzoni, E., Gentilini, C., Santandrea, M., Carloni, C. (2018) 'Effects of rising damp and salt  
723 crystallization cycles in FRCM-masonry interfacial debonding: Towards an accelerated laboratory test  
724 method', *Construction and Building Materials*, Vol. 175, pp. 225-238.
- 725 [14] Valluzzi, M.R., Modena, C., de Felice, G. (2014) 'Current practice and open issues in strengthening  
726 historical buildings with composites', *Materials and Structures*, Vol. 47, pp. 1971-1985.
- 727 [15] Tinazzi, D., Modena, C., Nanni, A. (2000) 'Strengthening of masonry assemblages with FRP rods and  
728 laminates', *International Meeting on Composite Materials, PLAST 2000, Proceedings, Advancing with  
729 Composites 2000*, pp. 411-418.
- 730 [16] Valluzzi, M. R., Binda, L., Modena, C. (2005) 'Mechanical behaviour of historic masonry structures  
731 strengthened by bed joints structural repointing', *Construction and Building Materials*, Vol. 19, pp.63-  
732 73.
- 733 [17] Turco, V., Secondin, S., Morbin, A., Valluzzi, M.R., Modena, C. (2006) 'Flexural and shear strengthening  
734 of un-reinforced masonry with FRP Bars', *Composites Science and Technology*, Vol. 66, pp.289-296.
- 735 [18] Casacci, S., Di Tommaso, A., Gentilini, C. (2015) 'Crack propagation in compression and mounted  
736 arrestors', *Key Engineering Materials*, Vol. 624, pp. 595-602.
- 737 [19] Borri, A., Castori, G., Corradi, M., Speranzini, E. (2011) 'Shear behavior of unreinforced and reinforced  
738 masonry panels subjected to in situ diagonal compression tests', *Construction and Building Materials*,  
739 Vol. 25, pp. 4403-4414.
- 740 [20] Akhaveissy, A.H., Milani, G. (2013) 'A numerical model for the analysis of masonry walls in-plane loaded  
741 and strengthened with steel bars', *International Journal of Mechanical Sciences*, Vol. 72, pp.13-27.
- 742 [21] Casacci, S., di Tommaso, A., Gentilini, C. (2016) 'Experimental investigation on pre-cracked masonry

- specimens repaired by bed joints structural repointing', *Brick and Block Masonry: Trends, Innovations and Challenges - Proceedings of the 16th International Brick and Block Masonry Conference, IBMAC*, pp. 2047-2054.
- [22] De Lorenzis, L., Teng, J.G. (2007) 'Near-surface mounted FRP reinforcement: An emerging technique for strengthening structures', *Composites Part B: Engineering*, Vol. 38, pp. 119-143.
- [23] Almeida, J.A.P.P., Pereira, E.B., Barros, J.A.O. (2015) 'Assessment of overlay masonry strengthening system under in-plane monotonic and cyclic loading using the diagonal tensile test', *Construction and Building Materials*, Vol. 94, pp. 851-865.
- [24] Incerti, A., Tilocca, A.R., Ferretti, F., Mazzotti, C. (2019) 'Influence of Masonry Texture on the Shear Strength of FRCM Reinforced Panels', *RILEM Bookseries*, Vol. 18, pp. 1623-1631.
- [25] Benedetti, A. (2019) 'Diagonal Compression Behaviour of Masonry Walls Reinforced with FRM Coatings', in: Aguilar R., Torrealva D., Moreira S., Pando M.A., Ramos L.F. (eds) *Structural Analysis of Historical Constructions*. RILEM Bookseries, Vol 18. Springer, Cham.
- [26] Giaretton, M., Dizhur, D., Garbin, E., Ingham, J.M., Da Porto, F. (2018) 'In-Plane Strengthening of Clay Brick and Block Masonry Walls Using Textile-Reinforced Mortar', *Journal of Composites for Construction*, Vol. 22, art. no. 04018028.
- [27] Menna, C., Asprone, D., Durante, M., Zinno, A., Balsamo, A., Prota, A. (2015) 'Structural behaviour of masonry panels strengthened with an innovative hemp fibre composite grid', *Construction and Building materials*, Vol. 1, pp. 111 – 121.
- [28] De Carvalho Bello, C.B., Cecchi, A., Meroi, E., Oliveira, D.V. (2017) 'Experimental and numerical investigations on the behaviour of masonry walls reinforced with an innovative sisal FRCM system' *Key Engineering Materials*, Vol. 747, pp. 190-195.
- [29] Li, T., N., Tumialan, J.G., Nanni, A. (2005) 'Analysis of unreinforced masonry concrete walls strengthened with glass fiber-reinforced polymer bars', *ACI Structural Journal*, Vol. 102, pp.569-577.
- [30] ACI 549 (2013). Design and construction guide of externally bonded FRCM system for concrete and masonry repair and strengthening.
- [31] Babaeidarabad, S., De Caso, F., Nanni, A. (2013) 'URM walls strengthened with fabric-reinforced cementitious matrix composite subjected to diagonal compression', *Journal of Composites for Construction*, Vol. 18:04013045.
- [32] Babaeidarabad, S., Arboleda, D., Loreto, G., Nanni, A. (2014) 'Shear strengthening of un-reinforced concrete masonry walls with fabric-reinforced-cementitious-matrix', *Construction and Building Materials*, Vol. 65, pp.243-253.
- [33] Yu, P., Silva, P., Nanni, A. (2017) 'In-plane Performance of unreinforced concrete masonry strengthened with prestressed GFRP bars', *Journal of Composites for Construction*, Vol. 21 (1), art. no. 04016064.
- [34] Dizhur, D., Griffith, M., Ingham, J. (2013) 'In-plane shear improvement of unreinforced masonry wall panels using NSM CFRP strips', *Journal of Composites for Construction*, Vol. 17, art. no. 04013010.
- [35] Ismail, N., Petersen, R.B., Masia, M.J., Ingham, J.M. (2011) 'Diagonal shear behaviour of unreinforced



780 masonry wallettes strengthened using twisted steel bars', *Construction and Building Materials*, Vol.  
781 25, pp. 4386-4393.

782 [36] Mahmood, H., Ingham, J. M. (2011) 'Diagonal compression testing of FRP-retrofitted unreinforced clay  
783 brick masonry wallettes', *Journal of Composites for Construction*, Vol. 15, pp. 810-820.

784 [37] Tumialan, J.G., Morbin, A., Nanni, A., Modena, C. (2001) 'Shear strengthening of masonry walls with FRP  
785 composites', *COMPOSITES 2001 Convention and Trade Show, Composites Fabricators Association*,  
786 Tampa (FL), October 3-6, 2001, 6 pp., CD-ROM.

787 [38] Turco, V., Secondin, S., Morbin, A., Valluzzi, M.R., Modena, C. (2006) 'Flexural and shear strengthening  
788 of un-reinforced masonry with FRP bars', *Composites Science and Technology*, Vol. 66, pp. 289-296.

789 [39] EN 772-1 (2011). Methods of test for masonry units – Part 1: Determination of compressive strength.

790 [40] EN 998-2 (2016). Specification for mortar for masonry - Part 2: Masonry mortar.

791 [41] Technical sheet (2018). [https://www.mapei.com/it/it/prodotti-e-soluzioni/prodotti/dettaglio/mape-antique-](https://www.mapei.com/it/it/prodotti-e-soluzioni/prodotti/dettaglio/mape-antique-mc)  
792 [mc](https://www.mapei.com/it/it/prodotti-e-soluzioni/prodotti/dettaglio/mape-antique-mc)

793 [42] EN 1015-11 (1999). Methods of test for mortar for masonry. Determination of flexural and compressive  
794 strength of hardened mortar.

795 [43] Technical sheet (2018). <http://www.mapei.com/public/COM/products/1071-planitophdmrestauro-gb.pdf>.

796 [44] Dalalbashi, A., Ghiassi, B., Oliveira, D.V., Freitas, A. (2018) 'Fiber-to-mortar bond behavior in TRM  
797 composites: Effect of embedded length and fiber configuration', *Composites Part B: Engineering*, Vol.  
798 152, pp. 43-57.

799 [45] ASTM C109 (2005). Standard test method for compressive strength of hydraulic cement mortars.

800 [46] ASTM D7205 (2016). Standard test method for tensile properties of fiber reinforced polymer matrix  
801 composite bars.

802 [47] Technical sheet (2018). [https://www.mapei.com/it/en/products-and-solutions/products/detail/mapegrid-g-](https://www.mapei.com/it/en/products-and-solutions/products/detail/mapegrid-g-220)  
803 [220](https://www.mapei.com/it/en/products-and-solutions/products/detail/mapegrid-g-220)

804 [48] Leone, M., Aiello, M.A., Balsamo, A., Carozzi, F.G., Ceroni, F., Corradi, M., Gams, M., Garbin, E.,  
805 Gattesco, N., Krajewski, P., Mazzotti, C., Oliveira, D., Papanicolaou, C., Ranocchiai, G., Roscini, F.,  
806 Saenger, D. (2017) 'Glass fabric reinforced cementitious matrix: Tensile properties and bond  
807 performance on masonry substrate', *Composites Part B: Engineering*, Vol. 127, pp. 196-214.

808 [49] Bramehuber, W., et al. (2016) 'Recommendation of RILEM TC 232-TDT: test methods and design of  
809 textile reinforced concrete: Uniaxial tensile test: test method to determine the load bearing behavior of  
810 tensile specimens made of textile reinforced concrete', *Materials and Structures/Materiaux et*  
811 *Constructions*, Vol. 49, pp. 4923-4927.

812 [50] Kalali, A., Kabir M. Z. (2012) 'Experimental response of double-wythe masonry panels strengthened with  
813 glass fiber reinforced polymers subjected to diagonal compression tests', *Engineering Structures*, Vol.  
814 39, pp.24-37.

815 [51] ASTM E519M (2015). Standard test method for diagonal tension (shear) in masonry assemblages.

816 [52] RILEM TC 76 – LUM (1991). Diagonal tensile strength tests of small wall specimens.

817 [53] Tomazevic, M. (1999). 'Earthquake-resistant design of masonry buildings', A. S. Elnashai & P. J. Dowling,  
818 eds., Imperial College Press.

819 [54] EN 1052-3. Methods of test for masonry. Part 3: Determination of initial shear strength; 2007.

820 [55] EN 1996-1-1. Eurocode 6 – Design of Masonry Structures – Part 1-1: General rules for reinforced and  
821 unreinforced masonry structures.

822 [56] D.M. 14 Gennaio 2008. Norme tecniche per le costruzioni (In Italian).

823 [57] Gentilini, C., D'Altri, A.M., Amato, M., Zanotti, P., Favaro, F., De Miranda, S. (2017) 'Salt attack effects  
824 on the shear behavior of masonry: Preliminary results of an experimental campaign', *Key Engineering*  
825 *Materials*, Vol. 747, pp. 512-517.

826 [58] Capozucca, R. (2011) 'Shear behaviour of historic masonry made of clay bricks', *Open Construction and*  
827 *Building Technology Journal*, Vol. 5, pp. 89–96.

828 [59] Vasconcelos, G., Lourenço, P.B. (2009) 'Experimental characterization of stone masonry in shear and  
829 compression', *Construction and Building Materials*, Vol. 23, pp. 3337-3345.

830

831